communications biology

A Nature Portfolio journal

Article

https://doi.org/10.1038/s42003-025-08841-y

Isoleucyl-tRNA synthetase depletion reveals vulnerabilities in *Mycobacterium abscessus* and *Mycobacterium marinum*

Dan Luo[1,2,10], Weile Xie[1,2,10], Chuan Wang[3], Yicheng Sun[4], Lu Zhang[5,6], Lan Qian[7], Jianming Zhang[8], Guanghui Dang[9], Siguo Liu[9] & Zhe Wang[1,2]

Mycobacterium abscessus and *Mycobacterium marinum* are nontuberculous mycobacteria that pose significant challenges due to their high drug resistance and persistence in hostile host environments. Aminoacyl-tRNA synthetases, such as isoleucyl-tRNA synthetase (IleRS), are crucial for protein synthesis and represent promising targets for antimicrobial development. This study investigates the role of IleRS in mycobacterial growth, metabolism, and pathogenesis using conditional gene silencing combined with microbiological, metabolomic, and transcriptomic analyses. Our findings indicate that IleRS is essential for mycobacterial growth and survival during infection. Depletion of IleRS disrupts branched-chain amino acid and pantothenate biosynthesis, leading to metabolic vulnerabilities and impaired persistence in macrophages and in mouse infection models. Based on our metabolic findings, we tested drug susceptibility and found that depletion of IleRS enhances sensitivity to pyrazinamide, highlighting a synergistic effect that could improve tuberculosis treatment. Furthermore, global gene set enrichment analysis reveals that IleRS knockdown might promote bacterial clearance by upregulating cholesterol metabolism and lysosome organization processes in macrophages. These results establish IleRS as a potential therapeutic target, offering new insights into reducing drug resistance and enhancing current treatment regimens for mycobacterial infections, including tuberculosis.

Over the past two decades, *Mycobacterium abscessus* (*M. abscessus*), a rapidly growing nontuberculous mycobacterium (NTM), has emerged as a significant and escalating threat to patients with cystic fibrosis (CF) and other chronic lung diseases[1]. The prevalence of *M. abscessus* infections among CF patients has increased worldwide, potentially driven by hospital-based person-to-person transmission and the emergence of globally dominant clones characterized by enhanced virulence and poor clinical outcomes[2]. Similarly, *Mycobacterium marinum* (*M. marinum*) is a well-known pathogenic mycobacterium for skin and soft tissue infections and is associated with fish and water. Among NTMs, it is one of the important pathogens that cause extra-respiratory human infections worldwide[3]. In addition, there is a specific scientific interest in *M. marinum* because of its genetic relatedness to *Mycobacterium tuberculosis* (M. *tuberculosis*) and because experimental infection of fish with *M. marinum* mimics the pathogenesis of tuberculosis[4–7]. These infections are notoriously difficult to treat, often resistant to standard therapies, and contribute to accelerated lung or skin and soft tissue damage, complicating clinical management, and impeding safe lung or tissue transplantation. This growing clinical challenge

[1]Shanghai Key Laboratory of Veterinary Biotechnology, School of Agriculture and Biology, Shanghai Jiao Tong University, Shanghai, China. [2]Collaborative Innovation Center of Agri-Seeds/School of Agriculture and Biology, Shanghai Jiao Tong University, Shanghai, China. [3]Key Laboratory of Medical Molecular Virology (MOE/NHC/CAMS), Shanghai Frontiers Science Center of Pathogenic Microorganisms and Infection, School of Basic Medical Sciences, Shanghai Medical College, Fudan University, Shanghai, China. [4]MOH Key Laboratory of Systems Biology of Pathogens, National Institute of Pathogen Biology, and State Key Laboratory of Respiratory Health and Multimorbidity, Center for Tuberculosis Research, Chinese Academy of Medical Sciences and Peking Union Medical College, Beijing, China. [5]Department of Microbiology, School of Life Science, Fudan University, Shanghai, China. [6]Shanghai Engineering Research Center of Industrial Microorganisms, Shanghai, China. [7]Institute of Translational Medicine, Shanghai Jiao Tong University, Shanghai, China. [8]Institute of Translational Medicine, Zhangjiang Institute for Advanced Study, Shanghai Jiao Tong University, Shanghai, China. [9]State Key Laboratory for Animal Disease Control and Prevention, Division of Bacterial Diseases, Harbin Veterinary Research Institute, Chinese Academy of Agricultural Sciences, Harbin, China. [10]These authors contributed equally: Dan Luo, Weile Xie. e-mail: wangz@sjtu.edu.cn

underscores the urgent need to develop novel therapeutic agents targeting nontuberculous mycobacterium infections.

Targeting protein synthesis has long been a critical focus in the development of antimicrobial agents[8]. Aminoacyl-tRNA synthetases (aaRSs) are essential enzymes in protein biosynthesis that catalyze the attachment of amino acids to their corresponding tRNAs through a specific two-step catalytic reaction[9]. Recent evidence indicates that GSK3036656, GSK656, and a novel series of 3-aminomethyl 4-halogen benzoxaboroles inhibit the leucyl-tRNA synthetase (LeuRS) of *M. tuberculosis*, demonstrating potent anti-*M. tuberculosis* and *M. abscessus* activities[10–12]. Similarly, mupirocin (MRC), a potent inhibitor of bacterial and archaeal isoleucyl-tRNA synthetase (IleRS) that spares its eukaryotic counterpart, which is clinically employed against methicillin-resistant *Staphylococcus aureus* (MRSA). These findings underscore the potential of aaRSs as promising targets for novel antibacterial agents.

Despite progress in the understanding of aaRSs, our knowledge of the biological consequences of their inhibition in mycobacteria remains limited, predominantly based on studies of conserved orthologous genes in other organisms. While comparative genomics has shown great potential in drug development, it may fail to account for the effects of ecological niches and selective pressures on gene evolution. Previous studies found that MRC does not inhibit the growth of mycobacteria, largely because mycobacterial IleRS exhibits eukaryote-like features, rendering it inherently resistant to MRC[13]. Furthermore, mycobacterial IleRS demonstrates a highly specific cross-species aminoacylation capability and an evolutionary trajectory distinct from other aaRSs in mycobacteria, highlighting the need to further investigate its biological role in supporting mycobacterial growth and infection.

In this study, we investigated the phenotypes of gene knockdown strains of NTM (including *M. marinum* and *M. abscessus*) with impaired isoleucyl-tRNA biosynthesis both in vitro and in vivo. Our findings demonstrate the critical role and effects of IleRS in the growth, metabolism, and infection regulation of NTM. Notably, IleRS deficiency resulted in metabolic inhibition of the pantothenate biosynthesis pathway in mycobacteria, which enhanced their sensitivity to pyrazinamide (PZA). These insights not only deepen our understanding of mycobacterial metabolic regulation but also offer a novel foundation for developing antibiotic combination strategies aimed at chronic and recurrent infections.

Results

IleRS depletion compromises *M. abscessus* and *M. marinum* growth and persistence in dormant and host infection states

We initially attempted to construct an IleRS knockout strain. However, as previously reported by Barbara Bosch et al.[14], IleRS is essential for mycobacterial viability, and we were unable to obtain knockout strains. To explore the role of IleRS in mycobacterial growth and infection, we utilized a CRISPR interference (CRISPRi) system, specifically from *Streptococcus thermophilus* (dCas9Sth1), to achieve targeted repression of *ileS* gene in *M. abscessus* and *M. marinum*[15]. By inserting sgRNA targeting *ileS* into the CRISPRi scaffold, we generated chemically inducible knockdown strains (IleRS_KD) in both *M. abscessus* and *M. marinum*, with gene repression controlled by anhydrotetracycline (ATC). The empty vector control (PLJR962_KD) was introduced into strains via electroporation (Fig. 1A and Supplementary Table S1). Quantitative Real-Time PCR (qRT-PCR) confirmed significant downregulation of *ileS* expression following exposure to the indicated concentrations of ATC, as shown in Supplementary Fig. S1A. The ATC concentrations used (500 ng/mL for *M. abscessus* and 200 ng/mL for *M. marinum*) were determined based on our dose–response curves and previous studies[16–18] (Supplementary Fig. S1B). Depletion of IleRS inhibited the growth of *M. abscessus* and *M. marinum* on agar plates and in standard liquid media. In contrast, control strains carrying the empty vector showed no significant changes in gene expression or growth (Fig. 1B, C).

Mycobacteria are capable of utilizing diverse host-derived carbon and nitrogen sources during infection, such as carbohydrates, fatty acids, amino acids, and cholesterol. These nutrients serve as key sources of carbon, nitrogen, and energy in the host environment[19,20]. Considering the essential role of IleRS in amino acid metabolism, we next evaluated how IleRS depletion affects *M. abscessus* and *M. marinum* survival under different nutrient conditions. In nitrogen- and carbon-defined minimal media[21,22], IleRS_KD strains of *M. abscessus* and *M. marinum* were unable to grow when glutamine (Gln), ammonium ($NH4^+$), or Asp served as the sole nitrogen sources, nor in glucose-containing media (Fig. 1D and Supplementary Fig. S1C, D). Notably, when cholesterol was the sole carbon source, *M. abscessus* IleRS_KD showed no significant growth defect compared to the control (PLJR962_KD), whereas *M. marinum* IleRS_KD did not grow (Fig. 2D and Supplementary Fig. S1C). To determine whether this difference was related to variable depletion efficiency, we quantified IleRS transcript levels by qRT-PCR following ATC induction under both cholesterol and standard 7H9 conditions. The results confirmed that IleRS depletion levels were comparable across conditions within each strain (Supplementary Fig. S1A), indicating that the observed growth differences were not due to differences in knockdown efficiency. These findings reveal a condition-dependent divergence in nutrient responsiveness between *M. abscessus* and *M. marinum*, possibly reflecting species-specific metabolic flexibility[23,24].

Mycobacterial infections often induce granuloma formation, where challenging conditions such as nutrient limitation, low pH, and ion imbalance drive bacteria into dormancy[25]. To mimic mycobacterial responses under dormancy-associated and host-derived stress conditions, we established nutrient deprivation, acidic, and multi-stress models based on previous studies[26–28]. Under dormancy and acidic conditions, IleRS depletion markedly inhibited the growth of *M. abscessus* and *M. marinum*. As nutrient availability and pH declined, IleRS depletion led to moderate growth impairment in *M. abscessus*, whereas *M. marinum* underwent a more pronounced growth arrest under the same conditions (Fig. 1D and Supplementary Fig. S2). Under multi-stress conditions, IleRS depletion significantly reduced survival rates of *M. abscessus* and *M. marinum* from day 2, with CFU counts decreasing by approximately 2 $\log_{10}$ for *M. abscessus* and nearly 3 $\log_{10}$ for *M. marinum* by day 10 (Fig. 2A). These findings indicate that IleRS depletion reduces the fitness of *M. abscessus* and *M. marinum* under dormancy-inducing and host-mimicking stress conditions.

To further evaluate the role IleRS under host-relevant conditions, we measured CFU counts in both RAW264.7 and PMA-activated THP-1 macrophages. The results showed that the *M. abscessus* IleRS_KD strain exhibited delayed growth during the 3-day infection period, with final CFU counts 0.5–0.8 $\log_{10}$ lower than the initial inoculum (Fig. 2B). In contrast, the *M. marinum* IleRS_KD strain demonstrated more obvious reductions in replication and survival within macrophages, with bacterial loads being at least 2–3 $\log_{10}$ lower than the control strains (Fig. 2C). These findings support our in vitro observation, particularly under host-relevant stress conditions, and reinforce the potential of IleRS as a therapeutic target for persistent mycobacterial infections.

Metabolic profiling reveals specific signatures of IleRS depletion

AaRSs play a crucial role in protein biosynthesis as they catalyze the formation of aminoacyl-tRNA. However, it remains unclear whether the growth inhibition caused by aaRS depletion results from direct metabolic bottlenecks or broader physiological effects. To explore this, we performed liquid chromatography-mass spectrometry (LC-MS) analysis of metabolic disturbances caused by IleRS silencing in *M. abscessus* prior to detectable reductions in cell viability. Our results demonstrated that IleRS depletion led to the accumulation of upstream intermediates in the IleRS-tRNA biosynthesis pathway, with five key metabolites of isoleucine biosynthesis showing significant accumulation (Fig. 3, Supplementary Fig. S3 and Data 2). This accumulation interfered with amino acid synthesis and utilization pathways, resulting in a broad elevation of amino acid pools, including phenylalanine, tryptophan, isoleucine, tyrosine, leucine, lysine and glycine. Notably, the branched-chain amino acid (BCAA) biosynthesis pathway was markedly upregulated, with a 12.9-fold increase in 2-ketoisovalerate (KIV) (Supplementary Fig. S3 and Supplementary Data 2).

Interestingly, KIV is also a precursor in the valine-to-pantothenate conversion pathway. Following the depletion of IleRS, we observed increased

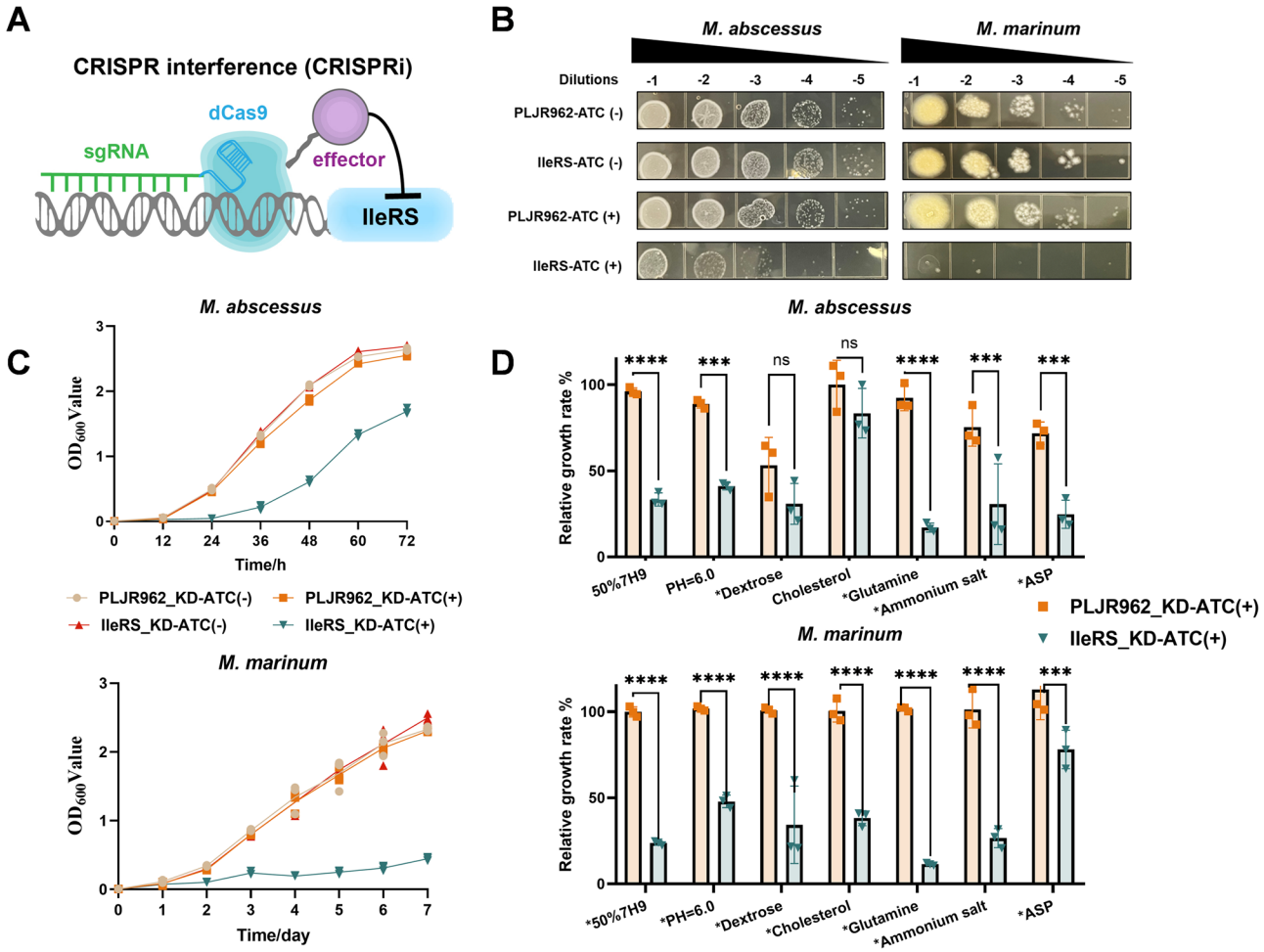

Fig. 1 | Essential role of IleRS in mycobacterial growth and survival revealed by CRISPRi silencing. A Schematic diagram of CRISPRi-mediated silencing of IleRS. **B** Growth of *M. abscessus* on 7H10 solid medium containing 500 ng/mL ATC at 37 °C and *M. marinum* on 7H10 containing 200 ng/mL ATC at 30 °C, starting from an initial dilution gradient of OD_{600} = 0.1. **C** Growth curves of *M. abscessus* and *M. marinum* in 7H9-OADC medium supplemented with 500 ng/mL ATC at 37 °C or 200 ng/mL ATC at 30 °C, respectively ($n = 3$). For the purpose of this study, "KD" refers to gene silencing via CRISPRi. **D** Silencing of IleRS in *M. abscessus* and *M. marinum* results in impaired carbon and nitrogen source utilization and reduced growth under acidic and nutrient-poor conditions ($n = 3$). The figure shows relative growth rates of empty vector strains (PLJR962_KD) and IleRS-silenced strains (IleRS_KD) during the logarithmic growth phase under ATC treatment compared to untreated conditions, expressed as OD_{600}^{+ATC} / OD_{600}^{-ATC}. For *M. abscessus*, relative growth rates were calculated at selected time points (36 h or 48 h), and for *M. marinum*, at 3d or 5d. The full set of observed time points and growth curves are shown in Supplementary Figs. S1 and S2. An text asterisk (*) indicates severe growth defects with failure to reach the normal plateau phase; absence of an asterisk indicates only a delay in reaching the plateau phase. Error bars represent mean ± SD. Statistical significance was determined by two-way ANOVA. Differences were considered statistically significant at $P < 0.05$ (*), $P < 0.01$ (**), $P < 0.001$ (***), and $P < 0.0001$ (****). "ns" denotes no significant difference.

flux of intermediates within this pathway. However, *M. abscessus* seemed to compensate for the reduced pantothenate flux by enhancing the conversion of aspartate to pantothenate. This suggests that upon IleRS depletion, BCAA intermediates from amino acid biosynthesis into pantothenate metabolism, thereby contributing to its inhibition. As previously described, the inhibition of the pantothenate pathway directly impacts coenzyme A synthesis, thereby potentially compromising energy production and lipid biosynthesis[29].

Moreover, IleRS depletion significantly downregulated metabolic fluxes related to nucleotide biosynthesis, the pentose phosphate pathway, and glycolysis, inducing a metabolically vulnerable state in *M. abscessus*. This disruption may explain why IleRS is essential for supporting growth under various nitrogen and carbon sources in vitro[30,31].

Targeting IleRS increases PZA susceptibility in mycobacteria

PZA remains a cornerstone drug in first-line tuberculosis (TB) therapy[32]. Although its standalone efficacy is modest—exhibiting only bacteriostatic effects or sometimes no activity against clinical strains[33,34]—PZA serves as an effective adjunct due to its unique ability to target semi-dormant bacilli[35]. Accordingly, PZA combined with isoniazid (INH) and rifampicin (RFP) forms the backbone of modern TB regimens, contributing to both shorter treatment durations and reduced relapse rates[36]. Despite the mechanism of action of PZA incompletely understood, Dillon et al. demonstrated that a pantothenate-deficient *M. tuberculosis* strain is sensitive to PZA and its active form, pyrazinoic acid (POA)[37,38]. Based on these findings and our metabolic data, we propose that the inhibition of pantothenate/coenzyme A biosynthesis caused by IleRS depletion might enhance the efficacy of PZA.

Given that PZA exhibits activity only under acidic or stress-inducing conditions, we investigated the synergistic effects of IleRS depletion and PZA under acidic and dormant state models. Under acidic conditions, PZA monotherapy exhibited negligible activity against *M. abscessus*. Notably, measurable antibacterial activity was observed only upon ATC-induced IleRS depletion, accompanied by a clear ATC dose–response relationship, indicating that the enhanced susceptibility is dependent on the extent of IleRS silencing (Fig. 4A). Similarly, IleRS depletion reduced the time to onset of PZA-associated bactericidal effect on non-replicative *M. abscessus* (Fig. 4B). This reduction was not due to additive effects, as 500 μg/mL of PZA alone

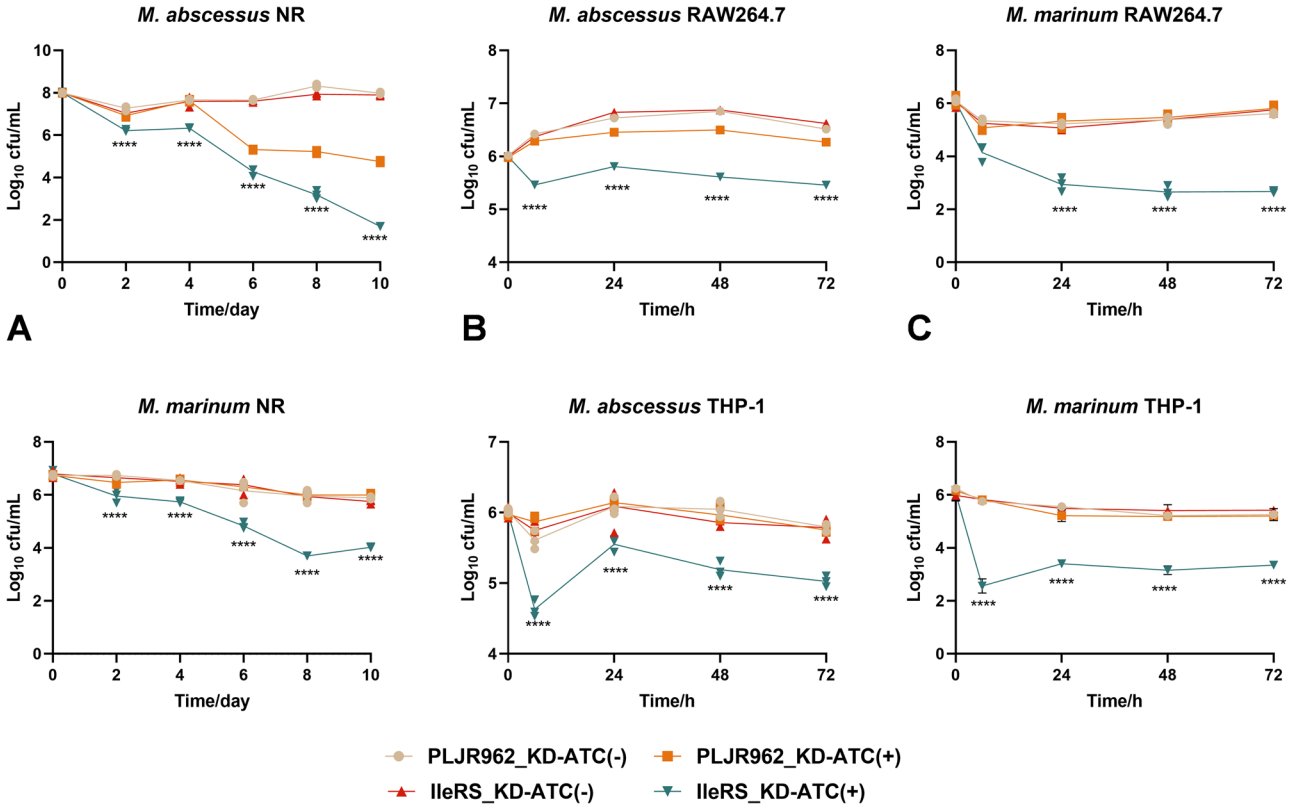

Fig. 2 | IleRS silencing compromises mycobacterial survival under stress and during macrophage infection. A Growth dynamics of IleRS-silenced and empty vector strains in NR medium under simulated multi-stress conditions, mimicking host immune pressures. Cultures were grown to an OD_{600} = 0.5 in 7H9, pelleted, and resuspended in NR medium with the indicated ATC concentrations for static incubation. Bacterial counts (CFU) were determined after 3–7 days by plating 10-fold serial dilutions on 7H10 agar ($n = 3$). **B** Survival of *M. abscessus* in RAW 264.7 and THP-1 macrophages infected at MOI = 1 with IleRS-silenced and empty vector strains. At 6, 24, 48, and 72 h post-infection, macrophages were washed, extracellular bacteria were removed with gentamicin (see Methods), cells were lysed with 0.01% SDS, and lysates were plated on 7H10 agar to quantify intracellular bacteria ($n = 3$). **C** Survival of *M. marinum* in RAW 264.7 and THP-1 macrophages under the same conditions as in (**B**). Both strains were pre-treated with ATC for 6 h and maintained under ATC throughout the infection period ($n = 3$). Error bars represent mean ± SD. Statistical significance was determined by two-way ANOVA. Differences were considered statistically significant at $P < 0.05$ (*), $P < 0.01$ (**), $P < 0.001$ (***), and $P < 0.0001$ (****). "ns" denotes no significant difference.

showed no anti-*M. abscessus* activity. To evaluate whether this interaction extends to other NTM species, we further evaluated its impact on *M. marinum*, demonstrating that IleRS depletion significantly enhanced the bactericidal effect of PZA on *M. marinum* (Fig. 4A, B). To determine whether this effect was specific to PZA, we systematically assessed the impact of IleRS depletion on the activity of commonly antimycobacterial drugs, including isoniazid (INH), rifampicin (RFP), ethambutol (EMB), pyrazinamide (PZA), amikacin (AMK), moxifloxacin (MXF), ethionamide (ETH) D-cycloserine (DCS), sodium para-aminosalicylic (PAS), linezolid (LZD), bedaquiline (BDQ), meropenem (MEM), clarithromycin (CLA) and clofazimine (CFZ). As shown in Fig. 4C, none of these antibiotics exhibited enhanced activity in the presence of IleRS knockdown, confirming that the sensitizing effect is specific to PZA and not due to a general loss of growth or fitness.

Finally, we evaluated the efficacy of combination in macrophage infection models. Compared to IleRS knockdown alone, the combined PZA treatment significantly reduced CFU in THP-1 and RAW264.7 cells, with reductions exceeding 1 $\log_{10}$ unit within 3 days (Fig. 4D). Collectively, these results reveal a conditionally druggable vulnerability unmasked by IleRS silencing and highlight the potential of combining aaRS-targeting strategies with metabolic adjuvants such as PZA or its analogs in the treatment of mycobacterial infections.

IleRS depletion reduces virulence of *M. abscessus* and *M. marinum* in mouse models

We previously demonstrated that *M. abscessus* and *M. marinum* rely on IleRS for sustained intracellular growth within macrophages. To further assess the impact of IleRS deficiency on pathogenic fitness, we conducted experiments using specific infection models in BALB/c mice.

M. abscessus is an opportunistic pathogen responsible for chronic pulmonary infections, particularly in individuals with cystic fibrosis or bronchiectasis[3]. Intranasal mouse models are widely employed to study pulmonary infections caused by mycobacteria[39–41]. In particular, Kim et al.[42] demonstrated that infecting immunocompetent mice with up to 1×10^4 CFU of *M. abscessus* ATCC 19977 provides a valuable model for evaluating antimicrobial interventions during infection progression. Following this model, we induced an acute pulmonary infection using high-dose *M. abscessus* challenge and monitored bacterial clearance over the first 7-day post-infection (Fig. 5A and Supplementary Fig. S4A).

Although lung CFU counts at day 0 and 3 post-infection remained comparable, mice infected with the IleRS_KD strain exhibited significantly milder lung pathology compared to those infected with the control PLJR962_KD strain (Fig. 5B, C). These findings indicate that, despite similar pulmonary bacterial loads, the IleRS_KD strain elicited reduced tissue pathology, highlighting the potential therapeutic value of targeting IleRS to mitigate infection-related lung injury. By day 7, pulmonary CFU counts in IleRS_KD-infected mice were reduced by 0.8 $\log_{10}$ compared to controls, indicating enhanced bacterial clearance. Additionally, we monitored CFU levels in the blood, as *M. abscessus* can be isolated from blood cultures in patients with bacteremia[43,44]. Blood CFU levels in the IleRS_KD group were over 1 $\log_{10}$ lower than in controls at both time points, suggesting that IleRS depletion significantly impaired the ability of *M. abscessus* to colonize and disseminate from the lung.

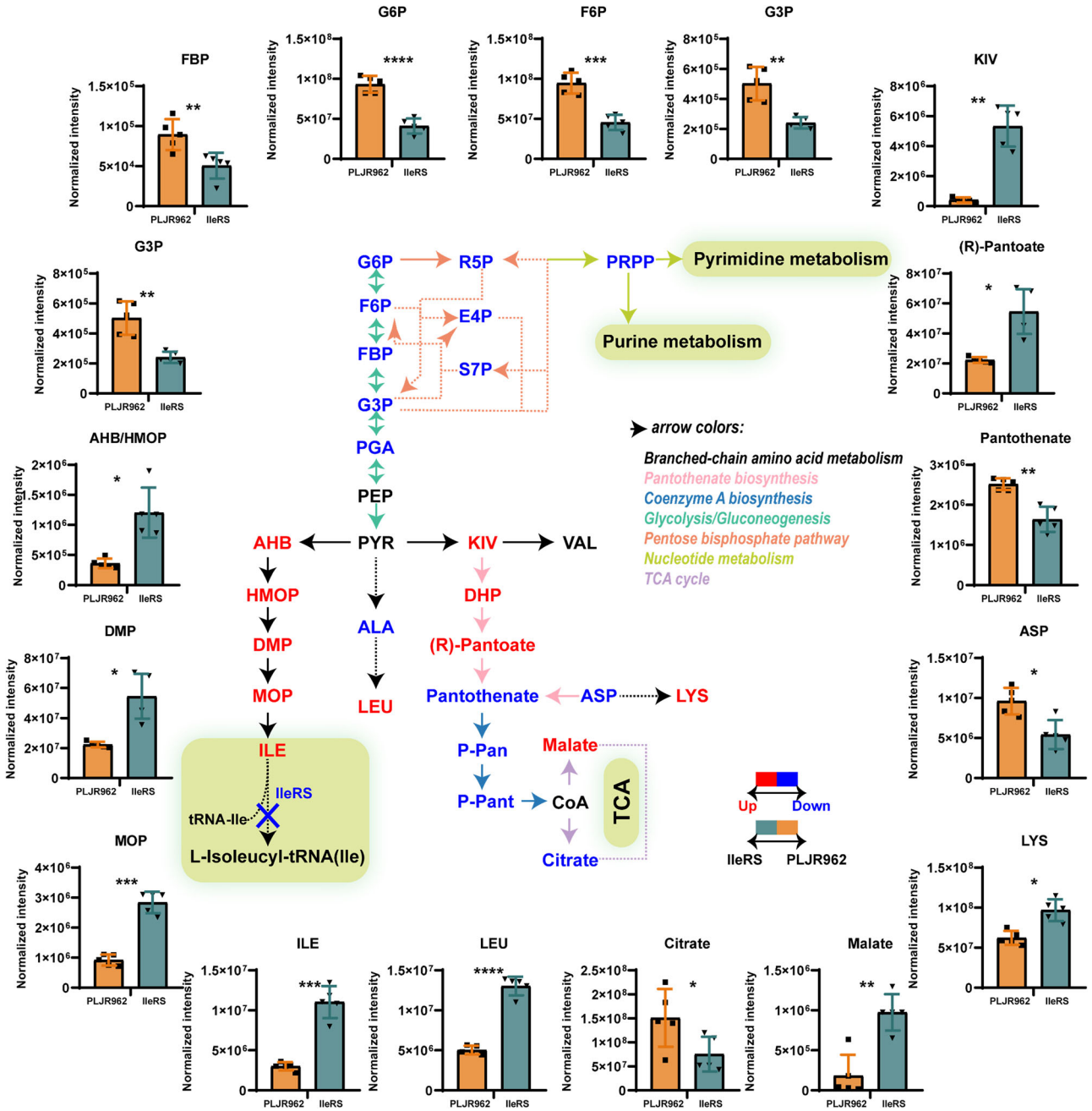

Fig. 3 | Metabolic alterations in *M. abscessus* due to IleRS silencing: disruption of branched-chain amino acid (BCAA), pantothenate, and coenzyme A pathways. Metabolic pathway analysis based on differentially expressed metabolites between IleRS-silenced (IleRS_KD) strains and empty vector strains (PLJR962_KD) under ATC treatment ($n = 5$). Representative bar graphs display normalized intensity values (mean ± SD; $n = 5$). Statistical significance was assessed by a two-tailed paired *t*-test ($n = 5$ pairs; thresholds: $P < 0.05$ (*), $P < 0.01$ (**), $P < 0.001$ (***), and $P < 0.0001$ (****)). Metabolites increased or decreased in response to IleRS silencing are highlighted in red and blue text, respectively. Metabolites that were undetectable or unchanged are shown in black. Colored arrows indicate pathway connectivity, with text colors matching the associated pathways. G6P glucose-6-phosphate, F6P fructose-6-phosphate, FBP fructose-1,6-bisphosphate, G3P glyceraldehyde-3-phosphate, PGA 3-phosphoglycerate, S7P sedoheptulose-7-phosphate, R5P ribose-5-phosphate, E4P D-erythrose-4-phosphate, PRPP 5-phosphoribosyl 1-pyrophosphate, PYR pyruvate, PEP phosphoenolpyruvate, KIV 2-ketoisovalerate, DHP 2-dehydropantoate, P-Pan 4′-phosphopantothenate, P-Pant pantetheine-4′-phosphate, AHB (S)-2-aceto-2-hydroxybutanoate, HMOP (R)-3-hydroxy-3-methyl-2-oxopentanoate, DMP (R)-2,3-dihydroxy-3-methylpentanoate, MOP (S)-3-methyl-2-oxopentanoate, ILE isoleucine, ALA alanine, LEU leucine, VAL valine, LYS lysine, ASP aspartate.

We next evaluated the effect of IleRS depletion on *M. marinum* virulence. *M. marinum* infections typically occur in cooler regions of the host's body surface[45]. Similar to *Mycobacterium leprae* (*M. leprae*), footpad infection model using *M. marinum* have previously been established in mice[46–48]. We adopted this approach, utilizing the footpad infection model to determine our experimental protocol (Supplementary Fig. S4B). Subsequently, we evaluated the virulence of *M. marinum* strains using the mouse footpad model (Fig. 5A). The control strain caused significant foot swelling by day 5, progressing to severe ulceration by day 10 post-infection (Fig. 5E). Histological analysis revealed extensive multifocal inflammation, characterized by lymphocyte and macrophage infiltration in the footpad. In contrast, mice infected with the IleRS_KD strain exhibited only mild swelling between 3 and 5 day post-infection, and disease progression was significantly limited. Inflammation and swelling were maintained at lower levels, with some mice

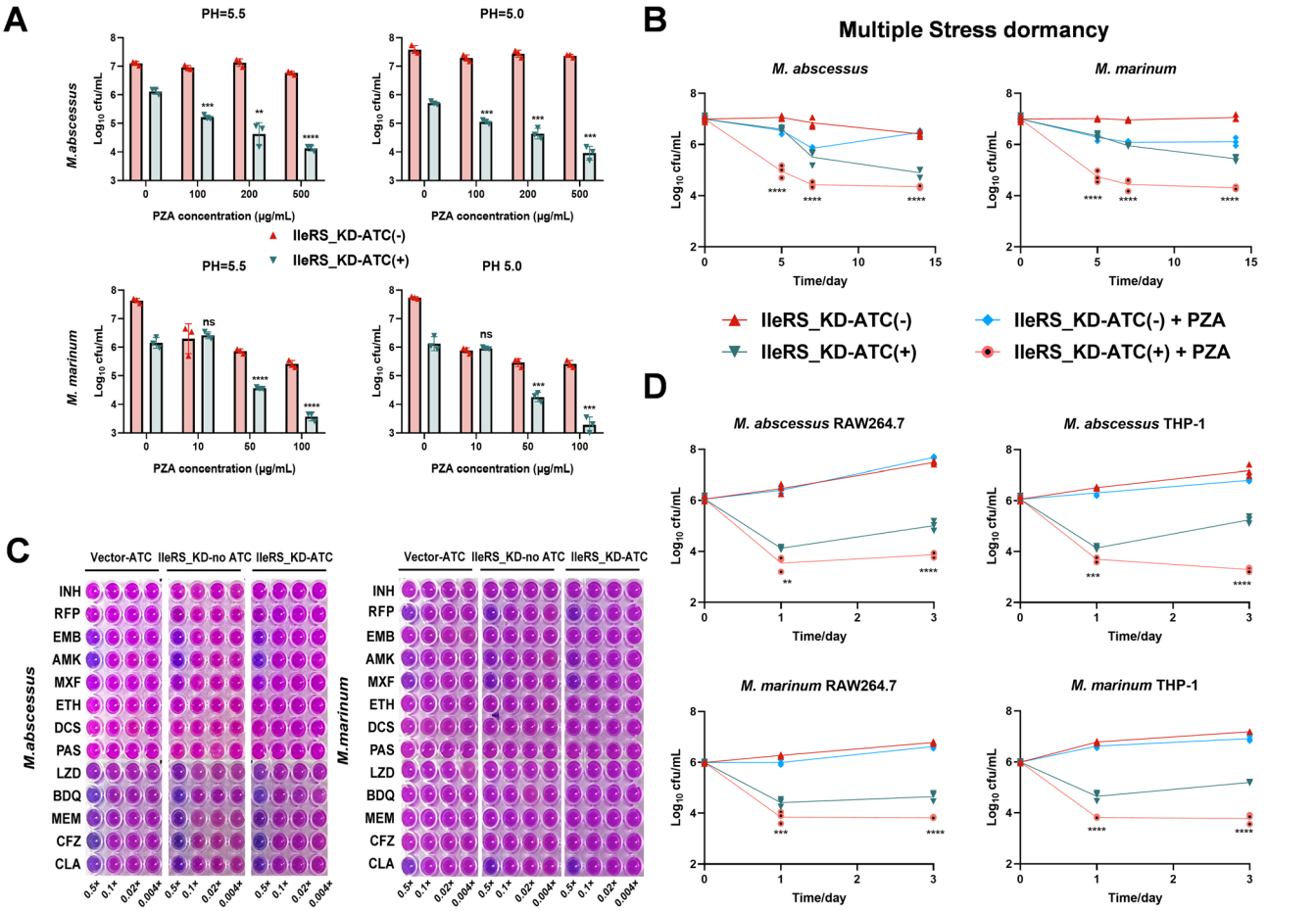

Fig. 4 | IleRS silencing enhances pyrazinamide (PZA) sensitivity in *M. abscessus* and *M. marinum*. IleRS-silenced (IleRS_KD) strains were compared with empty vector strains (PLJR962_KD) under four treatment conditions: untreated, PZA without ATC (no IleRS silencing), ATC alone (silencing control), and ATC + PZA. **A** Bar charts demonstrates the synergistic bactericidal effect of IleRS silencing and PZA on *M. abscessus* and *M. marinum* under acidic conditions (pH 5.0 and 5.5), with greater killing when ATC + PZA are combined than with either treatment alone ($n = 3$). **B** In the NR medium (non-replicating stress model; see Methods), IleRS silencing further enhances PZA activity, indicating a synergistic interaction under stress ($n = 3$). **C** alamarBlue microplate assay determining minimum inhibitory concentrations (MICs) of isoniazid (INH), rifampicin (RFP), ethambutol (EMB), pyrazinamide (PZA), amikacin (AMK), moxifloxacin (MXF), ethionamide (ETH), D-cycloserine (DCS), sodium para-aminosalicylic acid (PAS), linezolid (LZD), bedaquiline (BDQ), meropenem (MEM), clofazimine (CFZ), and clarithromycin (CLA). Drugs were tested at 0.004×–0.5× MIC. Empty vector strains and IleRS-silenced strains were tested with or without ATC induction. **D** Survival of *M. abscessus* and *M. marinum* in RAW 264.7 and THP-1 macrophage infected at MOI = 1. At 24 and 72 h post-infection, macrophages were washed, extracellular bacteria were removed with gentamicin (see Methods), cells were lysed with 0.01% SDS, and lysates were plated on 7H10 to quantify viable bacteria ($n = 3$). Error bars represent mean ± SD. Statistical significance was determined by two-way ANOVA. Differences were considered statistically significant at $P < 0.05$ (*), $P < 0.01$ (**), $P < 0.001$ (***), and $P < 0.0001$ (****). "ns" denotes no significant difference.

showing signs of recovery at the final observation point, aligning with histological findings (Fig. 5E). Further assessment of pathogenicity scores and CFU in the footpad reinforced the critical role of IleRS in *M. marinum* virulence. In the control group, pathogenicity scores and CFU units increased significantly over time, peaking on day 15. Conversely, the IleRS_KD group exhibited slower progression in pathogenicity, with CFU units decreasing markedly by at least 2 $\log_{10}$ units by day 15 (Fig. 5D).

Altogether, these findings confirm that IleRS is necessary for both *M. abscessus* and *M. marinum* survival of infection in mice.

Macrophage response to infection by IleRS-depleted strain

Because in vivo host–pathogen interactions often diverge from in vitro observations, characterizing the host transcriptional responses to IleRS depletion is essential for evaluating its therapeutic potential. We profiled RAW264.7 macrophages infected with the IleRS_KD or control strain using RNA-seq, identifying 44 differentially expressed genes (27 upregulated, 17 downregulated; Fig. 6A).

Upregulated genes included *Abca1*, a key cholesterol efflux transporter, consistent with prior findings that cholesterol metabolism is activated during *M. abscessus* infection[16]. In contrast, *Csf3* and *Defb42*, involved in neutrophil mobilization and antimicrobial defense, were significantly downregulated in IleRS_KD-infected cells (Supplementary Data 2).

GSEA revealed a functional reprogramming, enhancing pathways of lysosomal organization critical for bacterial degradation. Concurrently, innate immune sensing was suppressed, most notably via the cytosolic DNA-sensing pathway, together with core transcriptional and cell-cycle machinery (Fig. 6B)[49–53]. RT–qPCR validated the expression trends of selected RNA-seq targets (*Abca1*, *Abcg1*), and further quantified pro-inflammatory cytokines (*Il6*, *Tnf*, *Ifng*, *Il1b*), which were lower in IleRS_KD–infected macrophages (Fig. 6C). These findings highlight transcriptional signatures associated with altered inflammatory and metabolic responses upon IleRS depletion.

Discussion

Although the critical role of IleRS in ensuring the accurate incorporation of isoleucine during protein synthesis is well recognized, its underlying biochemical and physiological effects remain incompletely understood[40,54]. This study addresses this gap by integrating conditional gene silencing with

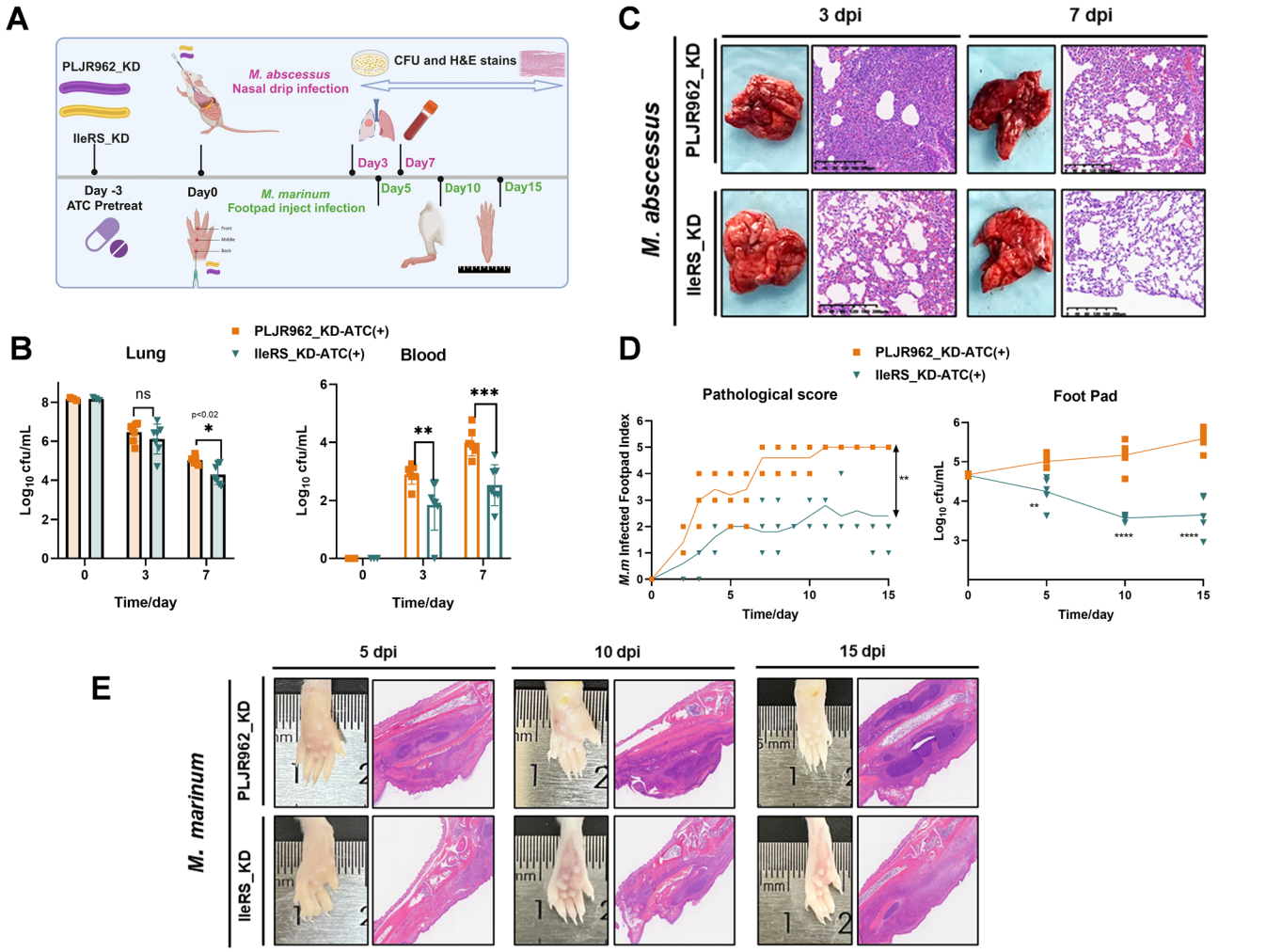

Fig. 5 | IleRS is critical for in vivo infection and pathogenesis of *M. abscessus* and *M. marinum*. **A** Experimental design: Empty vector strains (PLJR962_KD) and IleRS-silenced strains (IleRS_KD) were pre-treated with ATC for 3d prior to infection and maintained under ATC throughout the experiment (see Methods). In the *M. abscessus* model, BALB/c mice ($n = 9$) were intranasally inoculated with 1×10^8 CFU on day 0; in the *M. marinum* model, BALB/c mice ($n = 5$) were injected into the left hind footpad with 1×10^5 CFU on day 0. This figure was created using BioRender.com, with permission (https://BioRender.com/lz2lysa). **B** Bacterial loads of *M. abscessus* in the lung and blood at 0, 3 and 7d post-infection. Lungs were homogenized, serially diluted 10-fold, and plated on 7H10 agar supplemented with OADC to enumerate CFU ($n = 9$). Error bars represent mean ± SD. **C** Gross pathology and hematoxylin and eosin (H&E) staining of lung tissue at 3 and 7d post-infection with *M. abscessus*. **D** Left: Footpad pathology scores after *M. marinum* infection (index 0 = normal; 1 = non-inflammatory swelling; 2 = inflammatory swelling; 3 = swelling extending to hind foot; 4 = swelling extending to leg; 5 = wound burst with inflammation; see Methods). Right: Bacterial loads in footpads at 5, 10, and 15d post-infection, determined by homogenization, 10-fold serial dilution, and plating on 7H10 agar ($n = 5$). Error bars represent mean ± SD. **E** Gross pathology and H&E staining of footpad tissue at 5, 10, and 15d, showing progressive histopathological changes. Statistical significance was determined by two-way ANOVA. Differences were considered statistically significant at $P < 0.05$ (*), $P < 0.01$ (**), $P < 0.001$ (***), and $P < 0.0001$ (****). "ns" denotes no significant difference.

microbiological, metabolomic, and transcriptomic analyses, revealing the significance of IleRS in mycobacterial growth, persistence during in vivo infection, as well as virulence. Notably, our findings reveal that IleRS deficiency triggers metabolic vulnerabilities.

A key approach to studying host–pathogen interactions involves evaluating the phenotypic impact of specific enzyme knockouts, which can illuminate the ecological niche occupied by the pathogen within the host[40]. For instance, Hyungjin Eoh et al. reported that the deletion of isocitrate lyase (ICL) in *M. tuberculosis* reroutes the methylcitrate cycle into a metabolic "dead-end," depleting gluconeogenic precursors and demonstrating the potential of metabolomics in unraveling biochemically relevant pathways linked to specific phenotypes[55]. Our findings indicate that the metabolic vulnerability induced by IleRS deficiency is not solely due to the loss of a single enzyme's activity but also to multiple metabolic disruptions. These disruptions include: (i) increased levels of uncharged tRNA, leading to cellular amino acid starvation and enhanced amino acid flux, particularly due to the toxic accumulation of branched-chain amino acid (BCAA) intermediates; (ii) toxic accumulation of pantothenate biosynthesis intermediates, resulting in reduced pantothenate flux and inhibition of acetyl-CoA production; and (iii) significant downregulation of metabolic fluxes associated with nucleotide biosynthesis, the pentose phosphate pathway, and glycolysis. Similar to the response observed in *M. tuberculosis* treated with bedaquiline (BDQ), this low-energy vulnerable state leads to marked reductions in mycobacterial growth and virulence[56,57].

Interestingly, Swantje Reiß et al. reported that sub-inhibitory concentrations of MRC had minimal impact on the intracellular metabolome of *S. aureus* COL, with most core metabolites remaining unchanged under drug stress[58]. This observation differs markedly with our findings in mycobacteria, likely due to differences in bacterial physiology and the site of drug action. These discrepancies further highlight the imp of directly assessing IleRS perturbation in mycobacteria via gene depletion strategies. The metabolic plasticity of *M. tuberculosis* enables adaptation to diverse

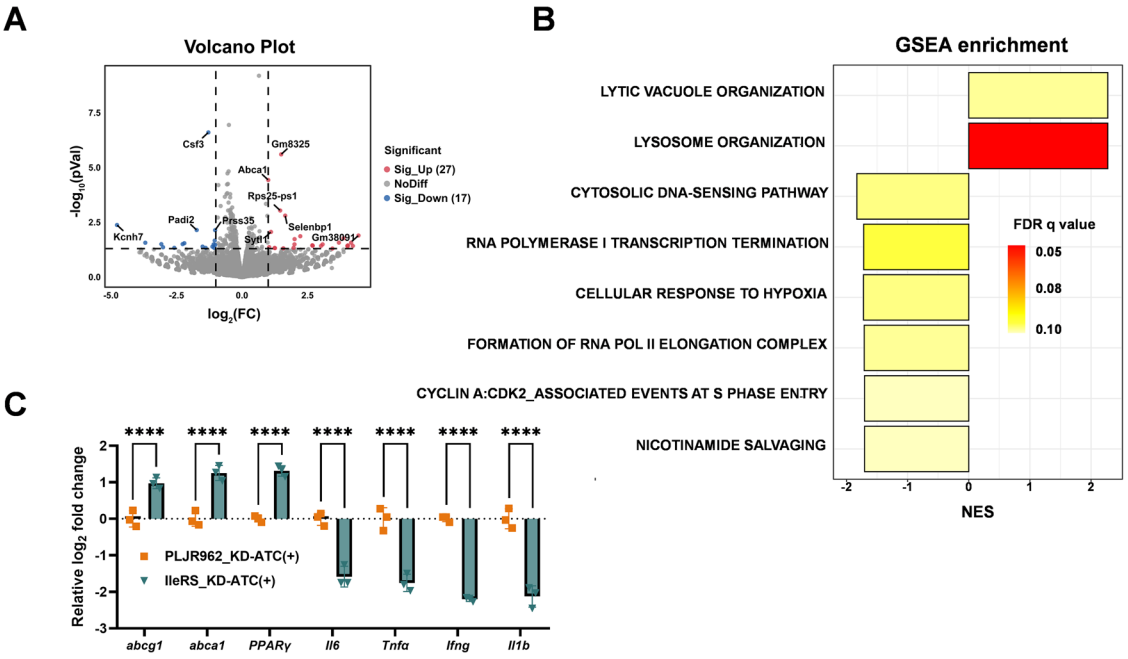

Fig. 6 | Transcriptome analysis of *M. abscessus* IleRS_KD infection in RAW 264.7 macrophages. **A** Volcano plot of differentially expressed genes (DEGs) identified using edgeR with a fold-change threshold of ≥2 or ≤0.5 and $P \leq 0.05$. Genes with significant upregulation (red) and downregulation (blue) are highlighted; larger $-\log_{10}(P)$ values indicate stronger significance. **B** Core enriched signaling pathways in macrophages infected with the IleRS_KD strain of *M. abscessus*, compared with empty vector strains (PLJR962_KD). Only pathways with NOM $P < 0.001$and FDR $q \leq 0.1$ are shown. **C** qRT-PCR validation of RNA-seq results, showing increased expression of *Abca1* and *Abcg1* (PPARγ-axis-related genes) and decreased *Il6*, *Tnf*, *Ifng*, and *Il1b* in macrophages infected with IleRS_KD compared with empty vector strains (PLJR962_KD). Error bars represent mean ± SD. Statistical significance was assessed by a two-tailed unpaired t-test; thresholds: $P < 0.05$ (*), $P < 0.01$ (**), $P < 0.001$ (***), and $P < 0.0001$ (****). "ns" denotes no significant difference.

host-derived stresses, including antibiotic exposure, and is a major contributor to prolonged treatment durations[59]. Targeting stress response and core metabolic pathways offers a rational strategy to enhance drug efficacy. In this study, IleRS depletion markedly increased susceptibility of both *M. abscessus* and *M. marinum* to PZA, especially under dormancy and macrophage infection conditions.

Although PZA itself exhibits limited clinical efficacy against NTM, recent medicinal chemistry efforts have produced multiple PZA derivatives and pantothenate analogs with improved cell permeability, acid stability, and antimicrobial potency. Pantothenamides, for example, disrupt CoA biosynthesis through metabolic hijacking[60]. Additionally, POA-derived inhibitors targeting PanD in *M. abscessus* have demonstrated promising enzymatic and whole-cell activity[61]. These advances reinvigorate interest in the PZA/POA axis as a druggable pathway in NTMs. These results underscore the therapeutic potential of targeting IleRS to expose stress-induced vulnerabilities in mycobacteria. Coupling aaRS inhibition with metabolic adjuvants may offer a rational strategy to overcome intrinsic drug resistance in recalcitrant NTM infections.

Studying host–pathogen interactions is critical for developing effective anti-infective drugs that disrupt essential pathways for pathogen survival in vivo. However, due to significant differences between in vivo and in vitro conditions, these pathways are often difficult to predict in laboratory studies[62,63]. Previous studies have identified foamy macrophages (FM) in both animal models of tuberculosis lesions and in granulomas from individuals with active tuberculosis[64,65]. Our findings show that IleRS deficiency in *M. abscessus* leads to upregulation of *Abcg1* and *Abca1* in macrophages. This modulation may mitigate immune-mediated tissue damage through anti-inflammatory effects and facilitate the clearance of mycobacterial infections[66,67]. Therefore, it is crucial to ascertain whether depletion of IleRS significantly impairs mycobacterial survival in vivo. Given the limited knowledge of *M. abscessus*, this remains a challenging question. Although the animal infection model of *M. abscessus* used in this study has limitations, it still provides valuable insights into the clearance of the IleRS_KD strain during acute infection. To gain a more comprehensive understanding of its role in vivo, future studies should evaluate its effects in immunodeficient mice. Additionally, the findings in foot pad infection with *M. marinum* also provide support for the importance of IleRS for mycobacterium. BCAA biosynthesis supplies essential substrates for branched-chain fatty acids, coenzyme A and pantothenate, and also mitigates intracellular BCAA accumulation by converting these amino acids into branched-chain keto acids (BCKAs)[40,68]. BCKAs may be routed into the tricarboxylic acid or methyl citrate cycles, providing alternative carbon and energy sources when external lipids or carbohydrates are limited[40,68]. Impaired BCKA metabolism has been associated with heightened M. tuberculosis sensitivity to diverse stresses and reduced virulence[69,70], and disruption of BCAA/BCKA pathways attenuates mycobacterial growth[71]. Consistent with these reports, our data indicate that loss of IleRS strongly compromises bacterial replication and survival in macrophages and in mouse acute lung and footpad infection models, supporting IleRS as a potential target for anti-mycobacterial therapy.

Previous studies have suggested that *M. tuberculosis* exhibits intrinsic resistance to MRC, likely due to its IleRS sharing greater sequence similarity with eukaryotic cytoplasmic homologs[13]. MRC inhibits bacterial IleRS by targeting conserved catalytic residues within the HIGH and KMSKS motifs, and its efficacy is highly sensitive to amino acid substitutions at these sites[72]. These observations imply that structural divergence in mycobacterial IleRS may impair binding of MRC and related compounds, limiting their antibacterial activity. Although this poses challenges for repurposing known IleRS inhibitors, IleRS remains a valid therapeutic target in NTM; rather, it highlights the need for alternative strategies that go beyond canonical active-site engagement[73,74].

Recent work in antimicrobial development has demonstrated that structurally conserved enzymes can still be selectively inhibited through allosteric mechanisms. For example, Kasbekar et al. discovered a cryptic

allosteric pocket in *M. tuberculosis* fumarate hydratase, enabling species-specific inhibition despite high conservation[75]. Zhong et al. leveraged structural differences in the SAM-binding site of bacterial TrmD versus eukaryotic Trm5 to develop TrmD-specific inhibitors[76]. Similarly, Andrade-Meirelles et al. designed P218 analogs that selectively inhibited DHFR from *M. avium* and *M. abscessus* while sparing the human enzyme[77]. These examples collectively support the feasibility of targeting mycobacterial IleRS via allosteric or conformationally selective inhibitors.

In silico modeling has recently suggested that taxifolin may inhibit both DNA gyrase and IleRS in mycobacteria[78]. To validate this, we constructed a *M. smegmatis* strain overexpressing *M. tuberculosis* IleRS (pMV261::*Mt*-IleRS) and exposed it to 100 μg/mL taxifolin. However, no evidence of target engagement was observed (Supplementary Fig. S5A, B). We then performed a differential whole-cell screen using the dual-strain approach described by Ramón Soto et al.[79]. Screening 2680 FDA-approved compounds against the overexpression and control (pMV261) strains also failed to yield any active hits (Supplementary Fig. S5C, D). These negative results likely reflect the low hit rate (<0.01%) and poor cell permeability frequently encountered in whole-cell screens targeting bacterial enzymes[80,81]. Despite the absence of validated inhibitors, we believe these findings are scientifically informative. Transparent reporting of negative results accelerates the validation process for IleRS as a drug target, and helps avoid redundant screening efforts[82–85]. Collectively, these data provide a strategic foundation for future mechanism-based or chemogenomic screening approaches aimed at identifying potent, mycobacteria-specific IleRS inhibitors.

In conclusion, this study systematically evaluates the essential role of IleRS in mycobacteria by simulating its depletion. Our findings uncover previously unrecognized connections between IleRS, BCAA, pantothenate metabolism, inflammation, and lipid metabolism in the host. These insights offer a new perspective on IleRS as a potential therapeutic target, offering the promise of reducing drug resistance in nontuberculous mycobacterium and *M. tuberculosis* and enhancing the efficacy of current mycobacterium treatment regimens.

Materials and methods

Bacterial culture and reagents

M. abscessus (ATCC19977) and *M. marinum* (M) strains were cultured in Middlebrook 7H9 broth (Difco™) supplemented with 10% acid-albumin-dextrose-catalase (ADC) (Becton Dickinson) or on Middlebrook 7H10 agar (Difco™) supplemented with 0.5% glycerol and 10% oleic acid-albumin-dextrose-catalase (OADC) (Becton Dickinson) at 37 °C or 30 °C under aerobic conditions.

All antibiotics used in this study—including isoniazid (INH), rifampicin (RFP), ethambutol (EMB), pyrazinamide (PZA), amikacin (AMK), moxifloxacin (MXF), ethionamide (ETH), D-cycloserine (DCS), sodium para-aminosalicylic acid (PAS), linezolid (LZD), bedaquiline (BDQ), meropenem (MEM), clofazimine (CFZ), doxycycline (DOX) and clarithromycin (CLA)—were obtained from Sangon Biotech (Shanghai, China). Anhydrotetracycline (ATC) was purchased from AstraZeneca (China) Co., Ltd.

Stock solutions were prepared according to compound solubility and manufacturer instructions. Specifically, INH, EMB, PZA, AMK, DCS, PAS, and MEM were dissolved in sterile distilled water; RFP, CFZ, BDQ, LZD, and ATC in dimethyl sulfoxide (DMSO); CLA in ethanol; and MXF in 0.1 M hydrochloric acid. All antibiotic solutions were sterilized using 0.22-μm syringe filters and stored at −20 °C until use.

CRISPR interference induction and in vitro growth conditions

To determine optimal induction conditions for CRISPR interference-mediated gene knockdown, dose–response assays were performed using IleRS knockdown strains of *M. abscessus* and *M. marinum*. Cultures of *M. abscessus* were treated with ATC at final concentrations of 0, 50, 100, 200, 500, and 1000 ng/mL, while *M. marinum* was exposed to 0, 50, 100, 200, and 500 ng/mL. Bacterial growth was assessed by measuring optical density at 600 nm (OD_{600}) at 12 or 24 h intervals for up to 3 days (*M. abscessus*) or 7 days (*M. marinum*), depending on the species' growth rates.

To simulate defined environmental stresses, modified Sauton medium was supplemented with either 2% glucose or 1% cholesterol as carbon sources, and with 1 g/L each of ammonium sulfate, glutamine, and aspartic acid as nitrogen sources. The pH was adjusted to 7.4 unless otherwise specified. Three in vitro model conditions were used: (i) a nutrient-limited model with 50% diluted 7H9 medium at pH 7.4; (ii) an acidic model using 7H9 adjusted to pH 6.0; and (iii) a multiple stress model using NR medium as described by Ben Gold et al.[86]. Log-phase cultures were centrifuged, washed with PBS, and resuspended in the appropriate test medium. Where indicated, ATC was added to a final concentration of 500 ng/mL for *M. abscessus* and 200 ng/mL for *M. marinum*, based on the results of dose–response optimization.

Mutant construction by CRISPR interference

CRISPR interference plasmids targeting IleRS in *M. abscessus* and *M. marinum* were constructed as our previously described[16]. The PLJR962 backbone was propagated in *Escherichia coli* under kanamycin selection, linearized by BsmBI digestion and gel-purified to receive sgRNA inserts. Guide sequences were chosen by locating the PAM motif 5′-NNAGAAG-3′ in promoter, 5′-UTR or coding regions and selecting the 20 nucleotides immediately downstream as the protospacer. Forward oligonucleotides included a 5′-GGGAG extension, while reverse oligonucleotides were reverse complements bearing a 5′-AAAC prefix and a terminal 3′C; all oligos were synthesized by Tsingke Biotechnology. Annealed duplexes with compatible overhangs were ligated into the BsmBI-digested backbone and multiplex assemblies followed established protocols; primer pairs are listed in Supplementary Table S1. Correct constructs were verified by Sanger sequencing using primer 1834-F (5′-TTCCTGTGAAGAGCCATTGA-TAATG-3′) and electroporated into competent *M. abscessus* and *M. marinum*. dCas9 expression was induced with the specified concentration of ATC to repress IleRS, RNA was collected at mid-log phase ($OD_{600} \approx 2.0$), and target transcript levels were quantified by qRT-PCR using primers provided in Supplementary Table S1.

Checkerboard assay and acidic PZA growth inhibition

To evaluate the synergistic effects of IleRS depletion with anti-tuberculosis drugs, checkerboard assays were performed using *M. abscessus* and *M. marinum* IleRS knockdown strains. Bacteria were seeded in 96-well plates containing two-fold serial dilutions of indicated antibiotics, either alone or in combination. Cultures were incubated at 37 °C (*M. abscessus*) or 30 °C (*M. marinum*) for 3–10 days, depending on species-specific growth rates. After incubation, 20 μL of 0.01% alamar blue solution was added to each well, and plates were incubated overnight. A color change from blue to pink was interpreted as an indication of bacterial growth. MIC values were defined as the lowest concentration with no visible color change. The fractional inhibitory concentration index (FICI) was calculated to evaluate synergistic, additive, or antagonistic interactions. All experiments were performed in triplicate.

To assess PZA susceptibility under acidic conditions, growth curve assays were performed in 7H9 medium adjusted to pH 5.0 or pH 5.5 and supplemented with indicated concentrations of PZA.

Macrophage infection

The macrophage cell lines RAW 264.7 and THP-1 were cultured in RPMI 1640 medium (Gibco, Thermo Fisher Scientific) supplemented with 10% heat-inactivated fetal bovine serum (FBS) (Gibco) at 37 °C with 5% CO_2. Macrophages were seeded in 6-well culture plates at a density of 1×10^6 cells/well. Infections of RAW 264.7 and THP-1 with *M. abscessus* or *M. marinum* were performed at a multiplicity of infection (MOI) of 1 for 4 h at 37 °C (for *M. abscessus*) or 30 °C (for *M. marinum*) with 5% CO_2. After infection, cells were washed twice with prewarmed 1 × PBS and treated with RPMI 1640 medium containing 500 μg/mL gentamicin to remove non-internalized mycobacteria.

At 6 h, 24 h, 48 h, and 72 h post-infection, cells were lysed with 0.2 mL of 0.01% SDS (dissolved in sterile 0.9% saline). Lysates were serially diluted and plated on 7H10 agar for colony-forming unit (CFU) enumeration. Cells infected in the CRISPR interference group were maintained in RPMI 1640 medium containing ATC (500 ng/mL for *M. abscessus* and 200 ng/mL for *M. marinum*) throughout the experiment. For pyrazinamide (PZA) treatment, a final concentration of 500 μg/mL PZA was used for *M. abscessus* and 100 μg/mL PZA for *M. marinum*.

Metabolomics profiling

For metabolomic profiling, *M. abscessus* IleRS_KD and PLJR962 strains cultures at OD600 = 0.5 were seeded onto 0.22-μM nitrocellulose filters atop 7H10 agar plates (supplemented with 500 μg/mL ATC) for 1 day. Bacteria were quenched in cold LC-MS–grade extract buffer (acetonitrile: methanol: water = 4:4:2). Mechanical lysis was performed using 0.1 mm silica beads in a Precellys tissue homogenizer, with continuous cooling at 4 °C. Protein concentration in the supernatant was measured using a Bradford assay kit (Beyotime, China).

Metabolites were separated using a Vanquish UHPLC system (Thermo Fisher, USA) equipped with an ACQUITY UPLC HSS T3 column and a gradient of water and acetonitrile containing 0.1% formic acid. The system was coupled to a Q Exactive Plus mass spectrometer (Thermo Fisher, USA), and data were acquired using Xcalibur 3.0 software (Thermo Fisher, USA). Raw data were processed with Progenesis QI v2.3 (Waters, UK) for peak picking, alignment, and normalization. Metabolite identifications were performed based on the HMDB database using Tracefinder (Thermo Fisher, USA). Statistical significance and differentially expressed metabolites (DEMs) were determined based on fold changes (≥1.5 or ≤0.66) and *p*-values (≤0.05). Statistical and pathway analyses were conducted using MetaboAnalyst 5.0 (http://www.metaboanalyst.ca/MetaboAnalyst/).

Macrophage transcriptome analysis

Murine RAW 264.7 macrophages infected with *M. abscessus* PLJR962 and IleRS_KD strains (MOI = 1) were collected 30 h post-infection using TRIzol (Invitrogen) for transcriptome purification. RNA-seq was performed on the Majorbio Bioinformatics Platform (Illumina), using Mus musculus (GRCM38.p6, http://asia.ensembl.org/Mus_musculus/Info/Index) as the reference genome. Functional annotation analysis of expressed genes and transcripts was conducted using the NR, Swiss-Prot, PFAM, COG, GO, and KEGG databases. Differential gene expression (DEG) analysis was performed using edgeR, with a screening threshold of fold change (FC) ≥ 2 or ≤0.5 and a *p*-value < 0.05. Gene Set Enrichment Analysis (GSEA) was used to analyze the enriched signaling pathways. Enrichment was considered significant with |NES|>1.5, NOM *p*-val <0.001, and FDR *q*-val ≤0.1. Matching RNA samples were used for quantitative PCR validation, with primer sequences provided in Supplementary Table S1.

Animal infection and sample collection

Female BALB/c mice (6–8 weeks old, specific pathogen-free), purchased from Spefo (Beijing) Biotechnology Co., Ltd., were acclimatised for 7 days before experiments in individually ventilated cages under controlled conditions (22 ± 2 °C, 50 ± 10% relative humidity, 12-h light/dark cycle) with ad libitum access to standard chow and water, and provided with nesting material and shelters for environmental enrichment.

Two infection models were established: a nasal infection model with *M. abscessus* and a footpad infection model with *M. marinum*. Mice were randomly allocated to groups using a random number table to ensure balanced distribution. For the *M. abscessus* model, $n = 9$ per group were intranasally inoculated with 1×10^8 CFU of PLJR962 or IleRS_KD strains, in a total volume of 40 μL, both pre-treated with anhydrotetracycline (ATC) for 3 days prior to infection. Anaesthesia was administered prior to inoculation using an approved anaesthetic agent. For the *M. marinum* model, $n = 5$ per group were injected into the left hind footpad with 1×10^5 CFU of PLJR962 or IleRS_KD strains, in a total volume of 20 μL using a 1 mL syringe, also pre-treated with ATC for 3 days. During the infection period, mice received 10% glucose–ATC water (5 mg/kg ATC per mouse) ad libitum.

Animals were monitored daily for body weight, posture, activity, and local inflammation. Euthanasia was performed by CO_2 inhalation at a flow rate of 20–30% of the chamber volume/min at predetermined time points: Day 3 and Day 7 for *M. abscessus* groups, and Day 5, Day 10, and Day 15 for *M. marinum* groups. For the *M. marinum* model, footpad swelling was assessed daily by a blinded animal technician trained in clinical scoring using the following system: 0 = normal; 1 = non-inflammatory swelling; 2 = inflammatory swelling; 3 = swelling extending to the hind foot; 4 = swelling extending to the leg; 5 = wound burst with inflammation. Humane endpoints were pre-defined as a score ≥5, severe ulceration, or >20% body weight loss; animals reaching these criteria were euthanised immediately. No animals met early euthanasia criteria.

Samples for CFU counts were obtained by plating organ homogenates on Middlebrook 7H10 agar plates supplemented with OADC, with incubation at 30 °C for 10–15 days for *M. marinum* or 37 °C for 6–10 days for *M. abscessus*. Portions of tissues were fixed in 10% neutral-buffered formalin, embedded in paraffin, sectioned, and stained with hematoxylin and eosin (H&E) for histopathological examination.

Ethics statement

All animal procedures were approved by the Animal Ethics Committee of Harbin Veterinary Research Institute (HVRI-IACUC-240426-02-GR), and we have complied with all relevant ethical regulations for animal use.

Whole-cell target-based screening

To identify potential IleRS inhibitors, a whole-cell screening was performed using *M. smegmatis* strains harboring either an empty vector (pMV261) or an overexpression construct encoding *M. tuberculosis* IleRS (pMV261::*Mt*-IleRS). A concentration of 5 μM for each compound from the FDA-approved drug library was selected to maximize hit identification sensitivity.

A standardized bacterial inoculum (1×10^5 CFU in 50 μL) was dispensed into 384-well clear flat-bottom plates using a Multidrop™ Combi dispenser (Thermo Scientific). Plates were sealed with parafilm, covered with aluminum foil to prevent light exposure, and incubated in humidified containers at 37 °C with 5% CO_2 for 48 h. Bacterial growth was assessed by OD_{600} measurement using a microplate reader (SpectraMax M5, Molecular Devices). Candidate hits were defined as compounds for which $\Delta OD_{600} \geq 50$ and OD_{600} (drug) ≈ OD_{600} of the 5 μM DOX control.

Statistics and reproducibility

All data are presented as the mean ± SD from at least three independent biological replicates. Data were analyzed using GraphPad Prism 8.0.1. Unless otherwise stated, comparisons were performed using two-way ANOVA. Statistical significance was defined as $P < 0.05$ (*), $P < 0.01$ (**), $P < 0.001$ (***), and $P < 0.0001$ (****). "ns" indicates no significant difference.

Reporting summary

Further information on research design is available in the Nature Portfolio Reporting Summary linked to this article.

Data availability

The RNA-seq data are available in the NCBI SRA under BioProject PRJNA1110605. The raw metabolomics data have been deposited in an online database. Access to these data is available through the following link: https://github.com/DanLuoCNS/CommunicationsBiology_Metadata. Numerical source data underlying all main-text figures are provided in Supplementary Data 1 (Excel, multi-tab). Full processed datasets for metabolomics and RNA-seq/GSEA are provided in Supplementary Data 2. Additional information or other data are available from the corresponding author upon reasonable request.

Received: 7 January 2025; Accepted: 3 September 2025;
Published online: 29 September 2025

References

1. Johansen, M. D., Herrmann, J.-L. & Kremer, L. Non-tuberculous mycobacteria and the rise of Mycobacterium abscessus. *Nat. Rev. Microbiol.* **18**, 392–407 (2020).
2. Cristancho-Rojas, C. et al. Epidemiology of Mycobacterium abscessus. *Clin. Microbiol. Infect.* **30**, 712–717 (2024).
3. Yan, S. et al. Overexpression of Rv2788 increases Mycobacterium stresses survival. *Microbiol. Res.* **195**, 51–59 (2017).
4. Ruley, K. M. et al. Identification of Mycobacterium marinum virulence genes using signature-tagged mutagenesis and the goldfish model of mycobacterial pathogenesis. *FEMS Microbiol. Lett.* **232**, 75–81 (2004).
5. Prouty, M. G., Correa, N. E., Barker, L. P., Jagadeeswaran, P. & Klose, K. E. Zebrafish-Mycobacterium marinum model for mycobacterial pathogenesis. *FEMS Microbiol. Lett.* **225**, 177–182 (2003).
6. Chan, K. et al. Complex pattern of Mycobacterium marinum gene expression during long-term granulomatous infection. *Proc. Natl. Acad. Sci. USA* **99**, 3920–3925 (2002).
7. Ramakrishnan, L. & Falkow, S. Mycobacterium marinum persists in cultured mammalian cells in a temperature-restricted fashion. *Infect. Immun.* **62**, 3222–3229 (1994).
8. Kwon, N. H., Fox, P. L. & Kim, S. Aminoacyl-tRNA synthetases as therapeutic targets. *Nat. Rev. Drug Discov.* **18**, 629–650 (2019).
9. Gupta, S. et al. Aminoacyl-tRNA synthetase - a molecular multitasker. *FASEB J.* **37**, e23219 (2023).
10. Tenero, D. et al. First-time-in-human study and prediction of early bactericidal activity for GSK3036656, a potent leucyl-tRNA synthetase inhibitor for tuberculosis treatment. *Antimicrob. Agents Chemother.* **63**, e00240–19 (2019).
11. Dong, W. et al. In vitro susceptibility testing of GSK656 against Mycobacterium species. *Antimicrob. Agents Chemother.* **64**, e01577–19 (2020).
12. Li, X. et al. Discovery of a potent and specific M. tuberculosis leucyl-tRNA synthetase inhibitor: (S)-3-(Aminomethyl)-4-chloro-7-(2-hydroxyethoxy)benzo[c][1,2]oxaborol-1(3H)-ol (GSK656). *J. Med. Chem.* **60**, 8011–8026 (2017).
13. Sassanfar, M., Kranz, J. E., Gallant, P., Schimmel, P. & Shiba, K. A eubacterial Mycobacterium tuberculosis tRNA synthetase is eukaryote-like and resistant to a eubacterial-specific antisynthetase drug. *Biochemistry* **35**, 9995–10003 (1996).
14. Bosch, B. et al. Genome-wide gene expression tuning reveals diverse vulnerabilities of M. tuberculosis. *Cell* **184**, 4579–4592.e24 (2021).
15. Blokpoel, M. C. J. et al. Tetracycline-inducible gene regulation in mycobacteria. *Nucleic Acids Res.* **33**, e22 (2005).
16. Xie, W., Luo, D., Wu, M., Sun, Y. & Wang, Z. The evaluation of Phenylalanine-tRNA ligase beta unit (PheT), as a potential target in Mycobacterium abscessus. *Tuberculosis***152**, 102626 (2025).
17. Kurepina, N. et al. CRISPR inhibition of essential peptidoglycan biosynthesis genes in Mycobacterium abscessus and its impact on β-lactam susceptibility. *Antimicrob. Agents Chemother.* **66**, e00093–22 (2022).
18. Nguyen, T. Q. et al. CRISPR interference-based inhibition of MAB_0055c expression alters drug sensitivity in Mycobacterium abscessus. *Microbiol. Spectr.* **11**, e0063123 (2023).
19. Baughn, A. D. & Rhee, K. Y. Metabolomics of central carbon metabolism in Mycobacterium tuberculosis. *Microbiol. Spectr*. **2**, MGM2-0026-2013 (2014).
20. Gouzy, A., Poquet, Y. & Neyrolles, O. Nitrogen metabolism in Mycobacterium tuberculosis physiology and virulence. *Nat. Rev. Microbiol.* **12**, 729–737 (2014).
21. Pandey, A. K. & Sassetti, C. M. Mycobacterial persistence requires the utilization of host cholesterol. *Proc. Natl. Acad. Sci. USA* **105**, 4376–4380 (2008).
22. Agapova, A. et al. Flexible nitrogen utilisation by the metabolic generalist pathogen Mycobacterium tuberculosis. *Elife* **8**, e41129 (2019).
23. Crowe, A. M. et al. The unusual convergence of steroid catabolic pathways in Mycobacterium abscessus. *Proc. Natl. Acad. Sci. USA* **119**, e2207505119 (2022).
24. van Wyk, R., van Wyk, M., Mashele, S. S., Nelson, D. R. & Syed, K. Comprehensive comparative analysis of cholesterol catabolic genes/proteins in mycobacterial species. *Int J. Mol. Sci.* **20**, 1032 (2019).
25. Sia, J. K. & Rengarajan, J. Immunology of Mycobacterium tuberculosis infections. *Microbiol. Spectr*. **7**, GPP3-0022-2018 (2019).
26. Gouzy, A., Healy, C., Black, K. A., Rhee, K. Y. & Ehrt, S. Growth of Mycobacterium tuberculosis at acidic pH depends on lipid assimilation and is accompanied by reduced GAPDH activity. *Proc. Natl. Acad. Sci. USA* **118**, e2024571118 (2021).
27. Luo, D., Xie, W. & Wang, Z. Curcumin enhances bedaquiline's efficacy against Mycobacterium abscessus: in vitro and in vivo evidence. *Microbiol. Spectr.* **13**, e0229524 (2025).
28. Xie, W., Luo, D., Soni, V. & Wang, Z. Functional characterization of MMAR_1296 in Mycobacterium marinum and its potential as a vaccine candidate. *Vaccine* **48**, 126720 (2025).
29. Evans, J. C. et al. Validation of CoaBC as a bactericidal target in the coenzyme a pathway of Mycobacterium tuberculosis. *ACS Infect. Dis.* **2**, 958–968 (2016).
30. Borah Slater, K. et al. One-shot 13 C15 N-metabolic flux analysis for simultaneous quantification of carbon and nitrogen flux. *Mol. Syst. Biol.* **19**, e11099 (2023).
31. DePas, W. H., Bergkessel, M. & Newman, D. K. Aggregation of nontuberculous mycobacteria is regulated by carbon-nitrogen balance. *mBio* **10**, e01715–e01719 (2019).
32. Heifets, L. & Lindholm-Levy, P. Pyrazinamide sterilizing activity in vitro against semidormant Mycobacterium tuberculosis bacterial populations. *Am. Rev. Respir. Dis.* **145**, 1223–1225 (1992).
33. Heifets, L., Higgins, M. & Simon, B. Pyrazinamide is not active against Mycobacterium tuberculosis residing in cultured human monocyte-derived macrophages. *Int. J. Tuberc. Lung Dis.* **4**, 491–495 (2000).
34. Sbarbaro, J. A., Iseman, M. D. & Crowle, A. J. Combined effect of pyrazinamide and ofloxacin within the human macrophage. *Tube Lung Dis.* **77**, 491–495 (1996).
35. Mitchison, D. A. The action of antituberculosis drugs in short-course chemotherapy. *Tubercle* **66**, 219–225 (1985).
36. Njire, M. et al. Pyrazinamide resistance in Mycobacterium tuberculosis: Review and update. *Adv. Med. Sci.* **61**, 63–71 (2016).
37. Shi, W. et al. Aspartate decarboxylase (PanD) as a new target of pyrazinamide in Mycobacterium tuberculosis. *Emerg. Microbes Infect.* **3**, 1–8 (2014).
38. Dillon, N. A., Peterson, N. D., Rosen, B. C. & Baughn, A. D. Pantothenate and pantetheine antagonize the antitubercular activity of pyrazinamide. *Antimicrobial Agents Chemother.* **58**, 7258–7263 (2014).
39. Nicola, F., Cirillo, D. M. & Lorè, N. I. Preclinical murine models to study lung infection with Mycobacterium abscessus complex. *Tuberculosis* **138**, 102301 (2023).
40. Shah, P. T., Tufail, M., Wu, C. & Xing, L. THP-1 cell line model for tuberculosis: a platform for in vitro macrophage manipulation. *Tuberculosis* **136**, 102243 (2022).
41. Lee, J.-Y. et al. Nucleotide-binding oligomerization domain 2 contributes to limiting growth of Mycobacterium abscessus in the lung of mice by regulating cytokines and nitric oxide production. *Front. Immunol*. **8**, 1477 (2017).
42. Kim, T. S. et al. Activity of LCB01-0371, a novel oxazolidinone, against Mycobacterium abscessus. *Antimicrobial. Agents Chemotherapy* **61**, https://doi.org/10.1128/aac.02752-16 (2017).

43. Suzuki, T. et al. Detection of Mycobacterium abscessus from blood cultures during treatment of interstitial pneumonia: a case study. *Rinsho Byori* **59**, 852–857 (2011).
44. Pavli, A. & Maltezou, H. C. Infectious complications related to medical tourism. *J. Travel Med.* **28**, taaa210 (2021).
45. Hashish, E. et al. Mycobacterium marinum infection in fish and man: epidemiology, pathophysiology and management; a review. *Vet. Q* **38**, 35–46 (2018).
46. Mor, N. & Levy, L. Importance of the footpad lesion in the mouse response to local inoculation of Mycobacterium marinum. *Ann. Inst. Pasteur. Microbiol.***136A**, 191–201 (1985).
47. Adams, L. B. Susceptibility and resistance in leprosy: studies in the mouse model. *Immunol. Rev.* **301**, 157–174 (2021).
48. Collins, F. M., Montalbine, V. & Morrison, N. E. Growth and immunogenicity of photochromogenic strains of mycobacteria in the footpads of normal mice. *Infect. Immun.* **11**, 1079–1087 (1975).
49. Ye, Y. et al. PPARγ ameliorates Mycobacterium tuberculosis H37Ra-induced foamy macrophage formation via the ABCG1-dependent cholesterol efflux pathway in THP-1 macrophages. *Front. Microbiol.* **13**, 829870 (2022).
50. Peyron, P. et al. Foamy macrophages from tuberculous patients' granulomas constitute a nutrient-rich reservoir for M. tuberculosis persistence. *PLoS Pathog.* **4**, e1000204 (2008).
51. Gago, G., Diacovich, L. & Gramajo, H. Lipid metabolism and its implication in mycobacteria-host interaction. *Curr. Opin. Microbiol.* **41**, 36–42 (2018).
52. Long, J. et al. Plasma membrane profiling reveals upregulation of ABCA1 by infected macrophages leading to restriction of mycobacterial growth. *Front. Microbiol.* **7**, 1086 (2016).
53. Chen, W. et al. The ABCA1-efferocytosis axis: a new strategy to protect against atherosclerosis. *Clin. Chim. Acta* **518**, 1–8 (2021).
54. Favrot, L., Amorim Franco, T. M. & Blanchard, J. S. Biochemical characterization of the Mycobacterium smegmatis threonine deaminase. *Biochemistry* **57**, 6003–6012 (2018).
55. Eoh, H. & Rhee, K. Y. Methylcitrate cycle defines the bactericidal essentiality of isocitrate lyase for survival of Mycobacterium tuberculosis on fatty acids. *Proc. Natl. Acad. Sci. USA* **111**, 4976–4981 (2014).
56. Koul, A. et al. Delayed bactericidal response of Mycobacterium tuberculosis to bedaquiline involves remodelling of bacterial metabolism. *Nat. Commun.* **5**, 3369 (2014).
57. Mackenzie, J. S. et al. Bedaquiline reprograms central metabolism to reveal glycolytic vulnerability in Mycobacterium tuberculosis. *Nat. Commun.* **11**, 6092 (2020).
58. Reiss, S. et al. Global analysis of the Staphylococcus aureus response to mupirocin. *Antimicrob. Agents Chemother.* **56**, 787–804 (2012).
59. Singh, N., Chauhan, A., Kumar, R. & Singh, S. K. Mycobacterium tuberculosis ketol-acid reductoisomerase down-regulation affects its ability to persist, and its survival in macrophages and in mice. *Microbes Infect.* **24**, 105000 (2022).
60. Butman, H. S., Kotzé, T. J., Dowd, C. S. & Strauss, E. Vitamin in the crosshairs: targeting pantothenate and coenzyme A biosynthesis for new antituberculosis agents. *Front. Cell Infect. Microbiol.* **10**, 605662 (2020).
61. Saw, W.-G. et al. Structural and mechanistic insights into Mycobacterium abscessus aspartate decarboxylase PanD and a pyrazinoic acid-derived inhibitor. *ACS Infect. Dis.* **8**, 1324–1335 (2022).
62. Pethe, K. et al. A chemical genetic screen in Mycobacterium tuberculosis identifies carbon-source-dependent growth inhibitors devoid of in vivo efficacy. *Nat. Commun.* **1**, 1–8 (2010).
63. Muñoz-Elías, E. J. & McKinney, J. D. M. tuberculosis isocitrate lyases 1 and 2 are jointly required for in vivo growth and virulence. *Nat. Med.* **11**, 638–644 (2005).
64. Kajiwara, C. et al. Apoptosis inhibitor of macrophages contributes to the chronicity of Mycobacterium avium Infection by promoting foamy macrophage formation. *J. Immunol.* **210**, 431–441 (2023).
65. Laval, T., Chaumont, L. & Demangel, C. Not too fat to fight: the emerging role of macrophage fatty acid metabolism in immunity to Mycobacterium tuberculosis. *Immunol. Rev.* **301**, 84–97 (2021).
66. Díaz, A. et al. Studies on the contribution of PPAR Gamma to tuberculosis physiopathology. *Front. Cell Infect. Microbiol.* **13**, 1067464 (2023).
67. Wu, J., Zhang, Y., Tang, H. & Ye, B.-C. MicroRNA-144-3p inhibits host lipid catabolism and autophagy by targeting PPARα and ABCA1 during Mycobacterium Tuberculosis infection. *ACS Infect. Dis.* **10**, 1654–1663 (2024).
68. Sharma, R., Keshari, D., Singh, K. S., Yadav, S. & Singh, S. K. MRA_1571 is required for isoleucine biosynthesis and improves Mycobacterium tuberculosis H37Ra survival under stress. *Sci. Rep.* **6**, 27997 (2016).
69. Singh, V. K. et al. Insertional inactivation of branched-chain α-keto acid dehydrogenase in Staphylococcus aureus leads to decreased branched-chain membrane fatty acid content and increased susceptibility to certain stresses. *Appl. Environ. Microbiol.* **74**, 5882–5890 (2008).
70. Glickman, M. S. & Jacobs, W. R. Microbial pathogenesis of *Mycobacterium tuberculosis:* dawn of a discipline. *Cell* **104**, 477–485 (2001).
71. Venugopal, A. et al. Virulence of Mycobacterium tuberculosis depends on lipoamide dehydrogenase, a member of three multienzyme complexes. *Cell Host Microbe* **9**, 21–31 (2011).
72. Nakama, T., Nureki, O. & Yokoyama, S. Structural basis for the recognition of isoleucyl-adenylate and an antibiotic, mupirocin, by isoleucyl-tRNA synthetase. *J. Biol. Chem.* **276**, 47387–47393 (2001).
73. Murima, P., McKinney, J. D. & Pethe, K. Targeting bacterial central metabolism for drug development. *Chem. Biol.* **21**, 1423–1432 (2014).
74. DeLaBarre, B., Hurov, J., Cianchetta, G., Murray, S. & Dang, L. Action at a distance: allostery and the development of drugs to target cancer cell metabolism. *Chem. Biol.* **21**, 1143–1161 (2014).
75. Kasbekar, M. et al. Selective small molecule inhibitor of the Mycobacterium tuberculosis fumarate hydratase reveals an allosteric regulatory site. *Proc. Natl. Acad. Sci. USA* **113**, 7503–7508 (2016).
76. Zhong, W. et al. Thienopyrimidinone derivatives that inhibit bacterial tRNA (Guanine37-N1)-methyltransferase (TrmD) by restructuring the active site with a tyrosine-flipping mechanism. *J. Med. Chem.* **62**, 7788–7805 (2019).
77. Andrade Meirelles, M. et al. Rational exploration of 2,4-diaminopyrimidines as DHFR inhibitors active against Mycobacterium abscessus and Mycobacterium avium, two emerging human pathogens. *J. Med. Chem.* **67**, 19143–19164 (2024).
78. Kozhikkadan Davis, C., Nasla, K., Anjana, A. K. & Rajanikant, G. K. Taxifolin as dual inhibitor of Mtb DNA gyrase and isoleucyl-tRNA synthetase: in silico molecular docking, dynamics simulation and in vitro assays. *Silico Pharm.* **6**, 8 (2018).
79. Soto, R. et al. Identification and characterization of aspartyl-tRNA synthetase inhibitors against Mycobacterium tuberculosis by an integrated whole-cell target-based approach. *Sci. Rep.* **8**, 12664 (2018).
80. Payne, D. J., Gwynn, M. N., Holmes, D. J. & Pompliano, D. L. Drugs for bad bugs: confronting the challenges of antibacterial discovery. *Nat. Rev. Drug Discov.* **6**, 29–40 (2007).
81. Anderson, D. E. et al. Comparison of small molecule inhibitors of the bacterial cell division protein FtsZ and identification of a reliable cross-species inhibitor. *ACS Chem. Biol.* **7**, 1918–1928 (2012).
82. Chalmers, I., Glasziou, P. & Godlee, F. All trials must be registered and the results published. *BMJ* **346**, f105 (2013).
83. De Angelis, C. et al. Clinical trial registration: a statement from the International Committee of Medical Journal Editors. *Lancet* **364**, 911–912 (2004).
84. Hayes, A. Key role of publication of clinical data for target validation. *Pharm. Res. Perspect.* **3**, e00163 (2015).

85. Nimpf, S. & Keays, D. A. Why (and how) we should publish negative data. *EMBO Rep.* **21**, e49775 (2020).
86. Gold, B., Warrier, T. & Nathan, C. A multistress model for high throughput screening against nonreplicating Mycobacterium tuberculosis. *Methods Mol. Biol.* **2314**, 611–635 (2021).

Acknowledgements

We thank Prof. Qian Gao (Fudan University) and the members of the Wang laboratory for helpful discussions and comments on the manuscript. We confirm that all individuals named in the Acknowledgements have agreed to be acknowledged. This work was supported by the National Key Research and Development Plans of China (No. 2021YFD1800401), the National Natural Science Foundation of China (No. 32070128), and the Shanghai Biomedical Science and Technology Support Special Project (No. 21S11900200).

Author contributions

Conceptualization: Dan Luo; Weile Xie. Methodology: Dan Luo; Guanghui Dang; Siguo Liu. Investigation: Dan Luo; Weile Xie; Chuan Wang; Yicheng Sun; Lu Zhang. Writing – original draft: Dan Luo; Weile Xie. Writing – review & editing: Chuan Wang; Yicheng Sun; Lu Zhang. Drug screening guidance: Lan Qian; Jianming Zhang. Supervision: Zhe Wang. Funding acquisition: Zhe Wang.

Competing interests

The authors declare no competing interests.

Additional information

Supplementary information The online version contains supplementary material available at https://doi.org/10.1038/s42003-025-08841-y.

Correspondence and requests for materials should be addressed to Zhe Wang.

Peer review information *Communications Biology* thanks the anonymous reviewers for their contribution to the peer review of this work. Primary Handling Editors: Karthika Rajeeve and Tobias Goris.